

Optics Letters

GaN/Ga₂O₃ avalanche photodiodes with separate absorption and multiplication structure

Rui Wang,¹ Zhenguang Shao,² Kaicheng Xu,¹ Ting Zhi,¹ Chunrong Gao,³ Junjun Xue,¹ and Jin Wang^{1,*}

Received 13 September 2023; revised 6 October 2023; accepted 7 October 2023; posted 9 October 2023; published 23 October 2023

This article proposes a new, to the best of our knowledge, separate absorption and multiplication (SAM) APD based on GaN/β-Ga₂O₃ heterojunction with high gains. The proposed APD achieved a high gain of 1.93×10^4 . We further optimized the electric field distribution by simulating different doping concentrations and thicknesses of the transition region, resulting in the higher avalanche gain of the device. Furthermore, we designed a GaN/β-Ga₂O₃ heterojunction instead of the single Ga₂O₃ homogeneous layer as the multiplication region. Owing to the higher hole ionization coefficient, the device offers up to a 120% improvement in avalanche gain reach to 4.24×10^4 . We subsequently clearly elaborated on the working principle and gain mechanism of GaN/β-Ga₂O₃ SAM APD. The proposed structure is anticipated to provide significant guidance for ultraweak ultraviolet light detection. © 2023 Optica Publishing Group

https://doi.org/10.1364/OL.505699

A wide-bandgap semiconductor Ga_2O_3 has arrived at the forefront of the field of ultraviolet light detection due to their inherent solar-blind characteristics, high critical electric field, high chemical, thermal stability, etc. Among the numerous isomers of Ga_2O_3 , β - Ga_2O_3 , which is the most stable phase, has been widely studied in the past decade. Various structures and designs of β - Ga_2O_3 photodetectors (PD) have been developed due to its proper bandgap (~4.9 eV), including photoconductive PDs, Schottky barrier PDs, and avalanche PDs (APDs) [1–3]. APDs, with ultrahigh internal gain, have the potential to become a major research focus in the future [4,5]. The research and development of Ga_2O_3 -based APDs are still in the early stages. The first report of Ga_2O_3 -based APD appeared in 2015 [6]. And now, Ga_2O_3 APD has achieved great performance improvements [3].

In APDs, we need p–n junctions to build high electric fields to meet the requirements of impact ionization [7]. Unfortunately, as an intrinsic n-type semiconductor, Ga_2O_3 is difficult to achieve efficient p-type conductivity. In contrast, controllable n-type doping has been demonstrated using group IV elements as dopants, including Si, Ge, and Sn [8–10]. One approach to overcome the challenge of p-type conductivity in Ga_2O_3 is to utilize p-GaN to form a p–n junction. Furthermore, GaN shows small

lattice mismatches with β -Ga₂O₃ (4.6% of (-201) β -Ga₂O₃ [11], 2.6% of (100) β -Ga₂O₃ [12]). More recently, high-quality GaN has been successfully grown on Ga₂O₃ via molecular beam epitaxy (MBE) [13] and metal-organic chemical vapor deposition (MOCVD) [14-16] and has been shown to have superior performance in field effect transistors, ultraviolet luminescence, and detection [16–18]. Moreover, a heterojunction structure can provide the necessary high electric field for impact ionization in APDs [19]. Compared to traditional p-i-n structures, the separate absorption and multiplication (SAM) structure can achieve higher gains and faster response times. The back-illuminated SAM structure facilitates holes to transport to the multiplication region and suppresses the impact ionization of electrons, resulting in a higher gain and superior noise characteristics. Additionally, it allows for a more flexible design of the polarization electric field. Those have been demonstrated through the development of SAM APDs based on AlGaN [20]. However, currently, there are no reports available on SAM APDs based on Ga₂O₃, and more studies are needed to explore the potential of Ga₂O₃ for SAM APDs and its performance in terms of gain or avalanche multiplication.

In this Letter, we employed Silvaco TCAD to investigate the gain characteristics of GaN/Ga_2O_3 back-illuminated SAM APDs. Meanwhile, we analyzed the effects of the doping concentration and thickness of the carrier transition region on APD properties. Furthermore, we improved the device structure by employing the GaN/Ga_2O_3 heterojunction as a multiplication region instead of a single Ga_2O_3 layer due to the higher hole ionization coefficient of GaN. At last, we figure out the working principle and gain mechanism of GaN/β - Ga_2O_3 SAM APD.

The designed GaN/Ga₂O₃ SAM APD structure is shown in Fig. 1(a), a 100 nm p-GaN layer with a doping concentration of $1\times10^{18}\,\mathrm{cm^{-3}}$ is employed as the top ohmic contact layer. The unintentionally doped $(1\times10^{16}\,\mathrm{cm^{-3}})$ absorption region and multiplication region both have a thickness of 200 nm. Due to the limited hole diffusion length of Ga₂O₃ (usually ~100 nm) [8], the thickness of the n-type transition region is restricted to below 100 nm. So, a 60 nm n-Ga₂O₃ layer with a doping concentration of $1\times10^{18}\,\mathrm{cm^{-3}}$ is employed as the carrier transition region to facilitate the transport of carriers. Figure 1(b) exhibits the electric field distribution of the proposed APD at

¹ College of Electronic and Optical Engineering & College of Flexible Electronics (Future Technology), Nanjing University of Posts and Telecommunications, Nanjing 210023, China

²School of Electronic and Information Engineering, Changshu Institute of Technology, Suzhou 215000, China

³B-soft LIMITED, Hangzhou 310052, China

^{*}jin@njupt.edu.cn

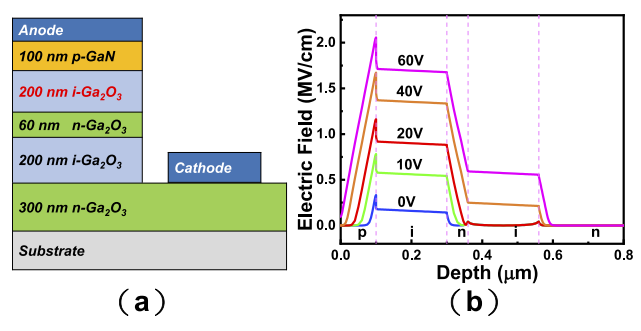


Fig. 1. (a) Structure diagram of GaN/Ga₂O₃ heterojunction p-i-n-i-n APD. (b) Calculated electric field distributions of the proposed APD at different reverse biases.

various biases. Due to the presence of a thin n-Ga₂O₃ layer, the absorption region maintains a low electric field. When a suitable reverse bias and photo are applied to the device, the photo will be absorbed in the absorption region to generate photogenerated electron-hole pairs. Under the effect of the electric field, the photogenerated holes and electrons will transport to opposite directions, resulting in only holes being involved in the impact ionization process. This pure hole injection of multiplication region in the SAM structure can effectively reduce the device noise and carrier recombination probability and improve the gain. In the simulation, we applied Poisson's equation and carrier continuity equation in the numerical procedures. The nonlinear algebraic system equations were solved by the Newton iteration method until self-consistent. Physical models can be classified into the following four types: mobility model (concentration-dependent and parallel electric field-dependent model), recombination model (Shockley-Read-Hall, Auger, and optical recombination model), carrier generation model (impact ionization and band-to-band tunneling model), and carrier statistical model (Fermi-Dirac statistical model). The ionization coefficients of Ga_2O_3 ($a_n = 2.16 \times 10^6 \text{ cm}^{-1}$, $b_n = 1.77 \times 10^7 \text{ V/cm}$, $a_p = 5.75 \times 10^6 \,\mathrm{cm}^{-1}$, $b_n = 1.77 \times 10^7 \,\mathrm{V/cm}$) and GaN ($a_n = 2.9 \times 10^7 \,\mathrm{V/cm}$) $10^8 \,\mathrm{cm}^{-1}$, $b_n = 2.37 \times 10^7 \,\mathrm{V/cm}$, $a_p = 1.3 \times 10^8 \,\mathrm{cm}^{-1}$, $b_p = 1.3 \times 10^8 \,\mathrm{cm}^{-1}$ 10⁷ V/cm) are extracted from Ref. [21,22]. The optical index coefficient of Ga₂O₃ was extracted from Ref. [23].

The simulated I–V and gain curves of the proposed GaN/Ga_2O_3 SAM APD are calculated under darkness and illumination of 256 nm UV light with a power of 8×10^{-5} W/cm², as shown in Fig. 2. The APD exhibits a broadband spectral response, as shown in the inset of Fig. 2. Two absorption peaks (~256 and 365 nm) are observed in spectral response corresponding to the cutoff wavelengths of Ga_2O_3 and GaN. The multiplication gain is calculated with the difference between the primary multiplied photocurrent and the multiplied dark current, which is normalized by the difference between the primary unmultiplied photocurrent and the unmultiplied dark current [24]. As the following formula shows

$$M = \frac{I_{\text{photo}} - I_{\text{dark}}}{I_{\text{u}}} \tag{1}$$

where $I_{\rm photo}$ and $I_{\rm dark}$ are the multiplied photocurrent and dark current, respectively. I_u is the unmultiplied mean current difference (0–50 V reverse bias). Since the low diffusion and generation–recombination current of wide-bandgap materials exceeds the calculated limits and the wider bandgap of Ga₂O₃ [25], the dark current exhibits great fluctuant when the reverse bias is less

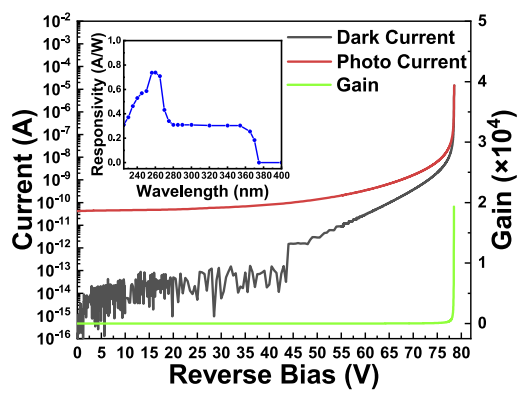


Fig. 2. I–V curves and multiplication gain of proposed APD. The inset shows the spectral responsivity of the APD.

than 50 V. When bias reaches 50 V, photocurrent and dark current increase exponentially with bias, meaning that the impact ionization process occurs. Both currents increase sharply when the reverse bias reaches 78.5 V, which means that the device experiences an avalanche breakdown. The gain increases sharply after avalanche breakdown, showing a hard Geiger mode breakdown. At last, the proposed APD achieved a max avalanche gain of 1.93×10^4 . Furthermore, we also calculated the avalanche gain under 365 nm UV light, and only a max gain of 2.0×10^3 was achieved. The photogenerated carriers generated at the GaN layer would not be accelerated by the electric field in the transit region due to Ga_2O_3 can't absorb the light of 365 nm, resulting in less energy of carriers during the avalanche multiplication process compared to the light of 256 nm and eventually achieving a smaller avalanche gain.

The introduction of the carrier transition region converts the conventional p-i-n structure into a SAM structure. Therefore, the proper design of the transition region has a significant impact on the performance of the device. To optimize the gain characteristics of the device, we conducted a study on the influence of different doping concentrations and thicknesses of the transition region, as shown in Fig. 3. The electric field intensity in the multiplication region increases concomitantly with the increase in doping concentrations or the increase in the thicknesses of the transition region (Figs. 3(a) and 3(c)), which induces the decrease of V_{BR} of APD, as shown in the red line of Figs. 3(b) and 3(d). Meanwhile, the excessively high doping of the transition region will decrease the electric field intensity in the absorption region and cause a high impurity scattering rate resulting in a decrease of carrier mobility. The excessively high thickness of the transition region will exacerbate the recombination, hindering the carriers transporting to the multiplication region. On the contrary, the excessively low doping and thickness of the transition region will cause the device to degenerate into a p-i-n structure, thus losing the ability to regulate electric fields. Subsequently, the variation trend of gain indicates the optimal thickness is around 70 nm and the optimal doping concentration is around 2×10^{18} cm⁻³, as shown in Figs. 3(b) and 3(d). When the transition region satisfies the optimal doping and thickness, a gain of 2.21×10^4 can be achieved.

Inspired by the higher hole ionization coefficient of GaN, we have replaced the single Ga_2O_3 multiplication region with a GaN/Ga_2O_3 heterojunction and designed an ionization-enhanced APD (IE-APD). For ease of distinction, we refer to the structure with a single Ga_2O_3 multiplication region as the

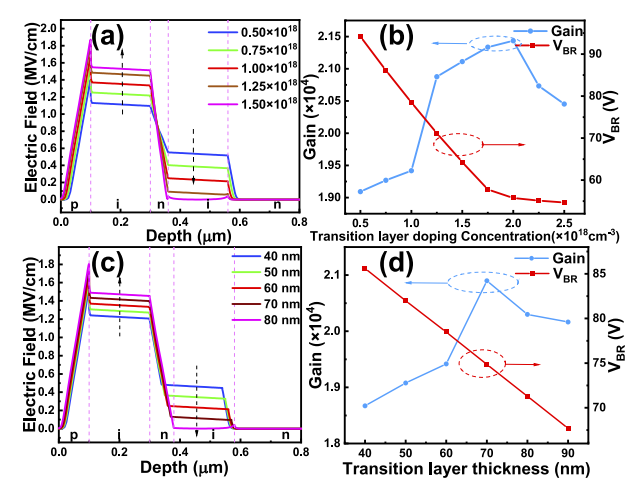


Fig. 3. (a) Electric field intensity versus doping concentrations of transition region at 40 V reverse bias. (b) V_{BR} and maximum gain versus doping concentration of transition region. (c) Electric field intensity versus thickness of transition region at 40 V reverse bias. (d) V_{BR} and maximum gain versus thickness of transition region.

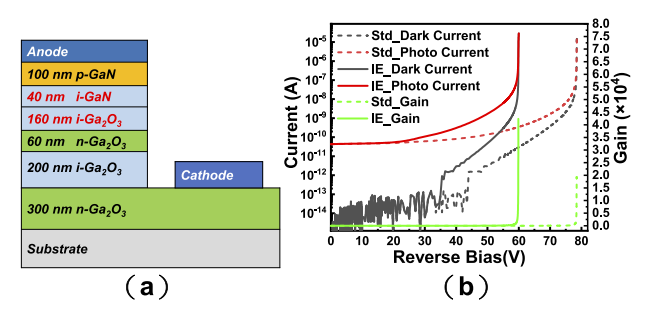


Fig. 4. (a) Structure diagram of GaN/Ga_2O_3 heterojunction ionization-enhanced p-i-n-i-n APD. (b) I–V curves and multiplication gain of ionization-enhanced (solid line) structure and standard (dashed line) structure.

standard APD (Std-APD). The IE structure is shown in Fig. 4(a). The IE-APD has a lower breakdown voltage compared to the standard APD since GaN requires a lower avalanche electric field compared with Ga_2O_3 , as shown in Fig. 4(b). The IE-APD achieves a max gain of 4.24×10^4 , which is 120% higher than the Std-APD. Similar to Std-APD, a smaller gain of 8.7×10^3 was achieved under the light of 365 nm. Furthermore, we also calculated various thicknesses of GaN in multiplication regions (80, 120, and 160 nm). We found that as the thickness of GaN increases, the gain increases while the $V_{\rm BR}$ decreases. When the multiplication region only has GaN, the max gain can be up to $\sim\!10^5$, and $V_{\rm BR}$ is only $\sim\!45\,\rm V$. This is easy to understand because GaN has a higher electric field in the breakdown state.

To further elucidate the gain mechanism of the GaN/Ga_2O_3 SAM-APD, we also calculated the diagram of carrier concentration distribution and band structure of IE-APD under zero bias and avalanche breakdown state ($-60\,V$), as shown in Fig. 5. From Fig. 5(a), we can observe that after the insert of the transit region, only the multiplication region depletes, while the whole intrinsic layer, which should have been fully depleted, does not. This phenomenon suggests that the introduction of the transition

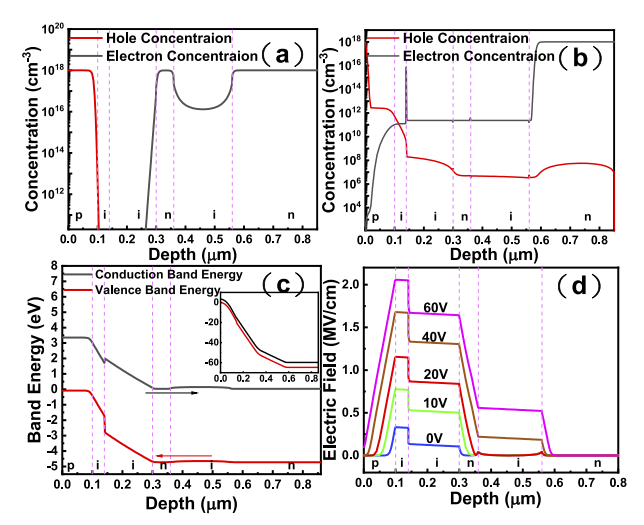


Fig. 5. Diagram of carrier concentration distribution of IE-APD at (a) 0 V and (b) -60 V. (c) Simulated band energy of IE-APD at 0 V. The inset exhibits the energy band diagram in the avalanche state. (d) Electric field intensity of IE-APD at various reverse biases.

region helps to separate the absorption region from the multiplication region. This separation is beneficial for the device's performance, as it allows for better carrier multiplication in the multiplication region. A distinct electric field was observed in the absorption region at $-40\,\mathrm{V}$ and extending to the bottom n-layer, meaning that the bottom n-layer has become a part of the depletion region (Fig. 5(d)). Meanwhile, the absorption region starts to absorb photons and generates photogenerated electron-hole pairs, which is manifested as an increase in photocurrent in Fig. 4(b). Figure 5(c) shows the energy band diagram of IE-APD, where the black and red arrow is the direction of electron and hole transport, respectively. Photogenerated holes can easily enter GaN from Ga₂O₃ thanks to the larger valence band offset. As can be seen in the inset, in the avalanche state, the energy band is flattened, and carriers can be transported smoothly. Figure 5(b) shows a severe accumulation of electrons located at the heterojunction interface, which would be the result of the polarization charge generated at the interface of GaN and Ga₂O₃. The hole concentration rises sharply in the i-GaN multiplication region and electron concentration in the multiplication region remains stable, meaning that only holes are involved in the avalanche multiplication process and the process only occurs in the multiplication region.

To illuminate the noise characteristics of IE-APD, we calculate the spectral densities of voltage fluctuations of APD at avalanche breakdown voltage. During the simulations, the total noise can be divided into four parts: generation–recombination (G–R) noise, electron diffusion (E-diff) noise, hole diffusion (H-diff) noise, and impact ionization (II) noise. From Fig. 6(a), device noise mainly originates from E-diff noise, which is an inevitable result of a large accumulation of electrons at the heterojunction interface (Fig. 5(b)). Figure 6(b) exhibits the various local noise source distributions in IE-APD at 1 MHz. We can find that the II noise is mainly concentrated in the multiplication region and e-diff noise is only significantly distributed at the interface of heterojunctions.

In summary, we designed a new GaN/Ga₂O₃ APD based on a separate absorption and multiplication structure. The proposed APD achieved a steep avalanche breakdown and a high

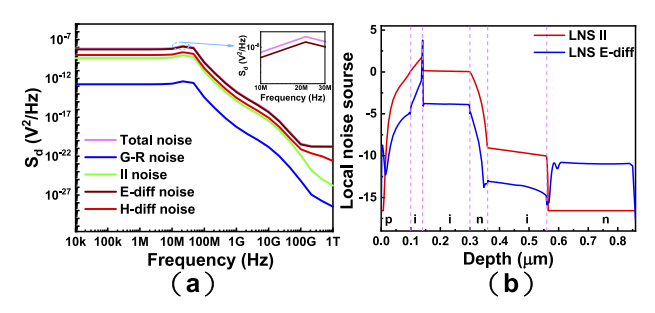


Fig. 6. (a) Spectral densities of voltage fluctuations for IE-APD at avalanche breakdown voltage. (b) Distribution of local noise sources in IE-APD.

gain. Through continuous simulation, the optimal concentration and thickness of the transmit layer have been achieved. Furthermore, we proposed an ionization-enhanced structure to further improve avalanche gain, achieving a remarkable gain improvement of 120%, reaching $4.24\times10^4.$ The calculated carrier concentration distribution and spectral densities of voltage fluctuations effectively validate the pure hole injection in the multiplication region and the suppression of electron-initiated multiplication. Our results indicate the exceptional potential of GaN/Ga_2O_3 APD in the field of single-photon detection in the future.

Funding. National Key Research and Development Program of China (2022YFB3605403); the National Natural Science Foundation of China (61974062, 62004104, 62104110); the Natural Science Foundation of Jiangsu Province (BK20200094, BK20210577); the Natural Science Foundation of the Jiangsu Higher Education Institutions of China (21KJB140020); the Project funded by China Postdoctoral Science Foundation (2023T160332).

Disclosures. The authors declare no conflicts of interest.

Data availability. Data underlying the results presented in this paper are not publicly available at this time but may be obtained from the authors upon reasonable request.

REFERENCES

- N. Liu, T. Zhang, and L. Chen, et al., IEEE Electron Device Lett. 43, 68 (2022).
- W.-Y. Kong, G.-A. Wu, and K.-Y. Wang, et al., Adv. Mater. 28, 10725 (2016).
- 3. Q. Zhang, N. Li, and T. Zhang, et al., Nat. Commun. 14, 418 (2023).
- 4. J. He, Q. Li, and P. Wang, et al., Opt. Express 28, 33556 (2020).
- 5. R. Xie, Q. Li, and P. Wang, et al., Opt. Express 29, 16432 (2021).
- 6. B. Zhao, F. Wang, and H. Chen, et al., Nano Lett. 15, 3988 (2015).
- H. Zhang, C. Huang, and K. Song, et al., Rep. Prog. Phys. 84, 044401 (2021).
- S. Modak, L. Chernyak, and A. Schulte, et al., Appl. Phys. Lett. 118, 202105 (2021).
- T. Ogawa, H. Nishinaka, and K. Shimazoe, et al., Jpn. J. Appl. Phys. 62, SF1016 (2023).
- 10. D. Guo, Y. Su, and H. Shi, et al., ACS Nano 12, 12827 (2018).
- M. M. Muhammed, M. Peres, and Y. Yamashita, et al., Appl. Phys. Lett. 105, 042112 (2014).
- E. G. Villora, K. Shimamura, and K. Kitamura, et al., Appl. Phys. Lett. 90, 234102 (2007).
- S. Ohira, N. Suzuki, and H. Minami, et al., Phys. Status Solidi (c) 4, 2306 (2007).
- Y.-P. Lan, Y.-C. Chen, and Y.-Y. Yeh, et al., Jpn. J. Appl. Phys. 58, 100908 (2019).
- M. M. Muhammed, N. Alwadai, and S. Lopatin, et al., ACS Appl. Mater. Interfaces 9, 34057 (2017).
- 16. W. Li, L. Guo, and S. Zhang, et al., CrystEngComm 22, 3122 (2020).
- S. Leone, R. Fornari, and M. Bosi, et al., J. Cryst. Growth 534, 125511 (2020).
- J. Wang, H. Guo, and C.-Z. Zhu, et al., IEEE Electron Device Lett. 41, 1052 (2020).
- H. Zhang, F. Liang, and K. Song, et al., Appl. Phys. Lett. 118, 242105 (2021).
- Z. G. Shao, X. F. Yang, and H. F. You, et al., IEEE Electron Device Lett. 38, 485 (2017).
- 21. F. Zhou, H. Gong, and M. Xiao, et al., Nat. Commun. 14, 4459 (2023).
- Q. Cai, M. Ge, and J. Xue, et al., IEEE Photonics J. 9, 6803507 (2017).
- T. Onuma, S. Saito, and K. Sasaki, et al., Jpn. J. Appl. Phys. 55, 1202B2 (2016).
- H. You, Z. Shao, and Y. Wang, et al., IEEE Photonics J. 9, 6802007 (2017).
- K. X. Dong, D. J. Chen, and H. Lu, et al., IEEE Photonics Technol. Lett. 25, 1510 (2013).